The Institute of Space and Astronautical Science
Report No. 601, October 1982

Thermal Behavior of Axially Grooved Heat Pipes aboard a Rocket

By

Masahide MURAKAMI*, Ryo TAKEUCHI*, Tomonao HAYASHI,
Tsuneo MACHIDA**, Seiichi KATO**, Yukio MATSUFUJI**
and Toshitaka HASUI**

(1, September, 1982)

Summary: Two axially grooved heat pipes, one using ammonia as the working fluid and another using freon 11, were launched aboard S-520 sounding rockets in January 1980 and in September 1981, respectively. The former was made of aluminum and the latter of aluminum alloy. N-eicosane was employed as a phase change heat sink material for both cases. They were fixed on the rocket axis with the condenser top. The heat pipes experienced several levels of varying acceleration such as large positive during the boosting period, small negative immediately after the burnout caused by the aerodynamic drag on the rocket, zero-gravity, and again positive while the re-entry. They responded to these situations. Such responses as dryout, recovery from the dryout with partial liquid blockage in the condenser section, and resumption of normal heat pipe operation were resulted from the dynamic behavior of the working fluid. The flight data were analyzed to understand the heat pipe performance and to investigate the dependence of the liquid motion on the body force and on the surface tension. The critical Bond number which gave a boundary between surface tension dominating and body force dominating regions was found to be the order of 10^{-3}.

1. Introduction

It is crucially important to investigate the zero-g performance of heat pipes for their applications to the thermal control of spacecraft. A number of onboard experiments by Deverall et al [1], Harwell et al [2], and Kirkpatrick [3] have been successfully undertaken. The International Heat Pipe Experiment was launched in 1974 (McIntosh, Ollendorf and Harwell [4], and Harwell, Quadrini, Sherman and McIntosh [5]). Experimental heat pipes to investigate the zero-g performance were also flown aboard rockets (Galzin [6], and Savage et al [7]). These experiments have, indeed, given us a lot of data on zero-g performance. However, it has also been indicated in some reports that the transient behavior to zero-g operation and the dynamic response of the working fluid to varying acceleration should be investigated for a full understanding of onboard performance.

The primary purpose of our experiments was to investigate such thermal and dynamic behaviors of axially grooved heat pipes, as well as to examine the zero-g performance. Two axially grooved heat pipes were launched by single-stage S-520 rockets in January 1980 and in September 1981, respectively, which have been recently developed by the Institute. An aluminum heat pipe using ammonia as the working

* Institute of Structural Engineering, University of Tsukuba.
** NEC Nippon Electric Co., Ltd.

fluid was flown at the first opportunity, and an aluminum alloy pipe using freon 11 was done at the second. The data during the flight were transmitted by a PCM telemetry and recorded on magnetic tapes for subsequent analysis. The first one provided us data concerning dryout and recovery coupled with negative acceleration, and the zero-g operation, though the telemetry data was received only until 243 sec, just before the apogee, because of a failure of the central power supply system of the rocket. At the second flight, all the components worked satisfactorily and the data were perfectly received for about 450 sec.

We are going to describe, for the most part, the second experiment in this report. The first will be referred to if necessary. Some discussion is also presented here on the criterion for deciding the fluid behavior depending on whether surface tension or acceleration forces dominate.

2. Vehicle and Flight Record

Each rocket was launched from Kagoshima Space Center, Institute of Space and Astronautical Science, in January 1980 and in September 1981, respectively. The schematic illustration of the vehicle, S-520 Rocket, is shown in Fig. 1 for the second experiment. It has a 524-mm diameter can and is powered by a solid fuel engine which develops 18 ton of thrust. The characteristic parameters for the first are basically same as the second except the launching weight 2112 kg (2311 kg for the second) and the total length of the rocket 7.94 m (9.01 m for the second). The second mission included the test of the recovery system which resulted in perfect success. However, our heat pipe experiment was not included in that section.

The flight trajectory, the spin rate and the attitude of the rocket are given in Fig. 2. The rocket attitude was expressed here by the angle of the rocket axis measured from the standard direction, azimuth angle of 175 deg and the elevation angle of 46 deg,

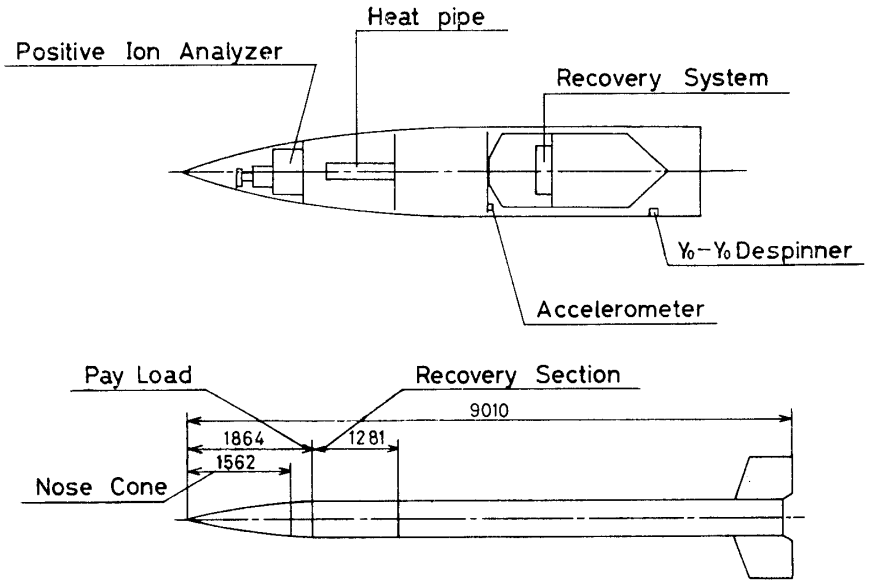

Fig. 1. Sς20-4 Rocket; whole view and payload section.

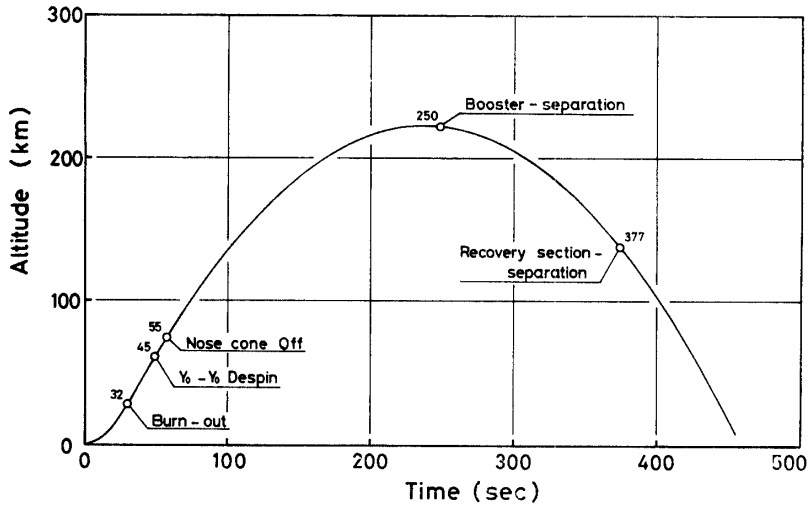

2-a. The flight trajectory.

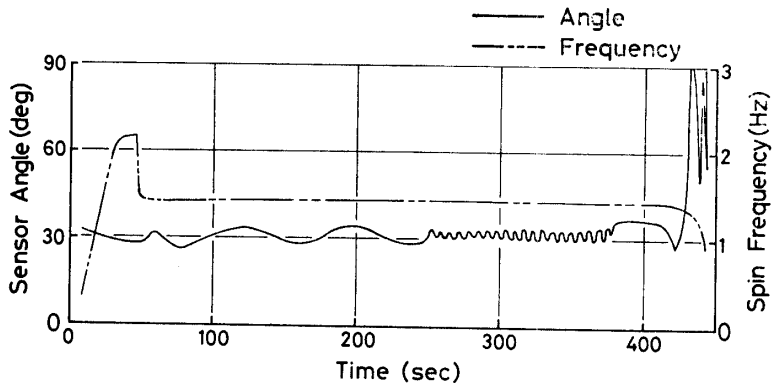

2-b. The spin rate and vehicle attitude.

Fig. 2. The Flight records.

which was measured by a geomagnetic attitude sensor. The rocket started to spin aerodynamically in order to stabilize the attitude due to small cant of four fins. The motor burnout was at 32 sec, when the spin rate reached about 2.2 Hz. Then, the yo-yo despin was activated at 45 sec to reduce the rate down to 1.4 Hz. The nose cone was removed for optical observations at 55 sec. Minor coning motion was detected during the free flight as seen in Fig. 2-b. The axial component of the acceleration, G_{ax}, is shown in Fig. 3-a. The axes of the rocket and the pipe just coincided with each other. It reached the maximum, 14.7 g_0, at 26.5 sec (18 g_0 for the first because of its light weight) and then rapidly decreased nearly to zero. Immediately after the burnout, the rocket suffered drag force because of the residual atmosphere and it produced negative acceleration reaching $-0.3\ g_0$ at its extreme at 32 sec, as seen from Fig. 3-b. Where g_0 represents the gravitational acceleration. It diminished down to zero gradually, and finally the absolute value of the axial component became less than $10^{-3}g_0$. This state may be regarded as zero-g for the present experiment. The booster and the recovery system were separated from the payload section at 250 sec

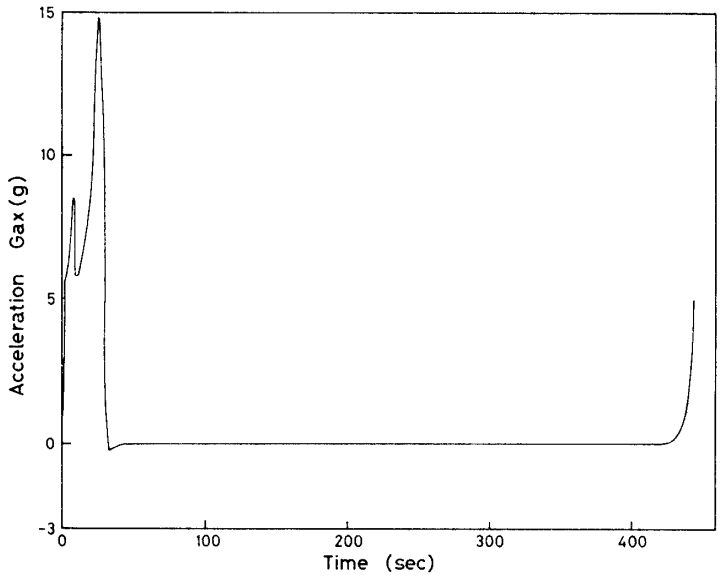

3-a. 0 through 485 sec.

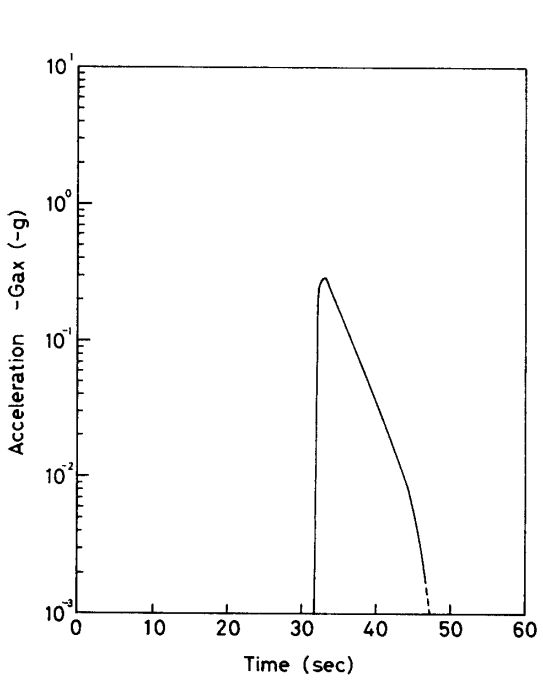

3-b. Negative-acceleration-period.

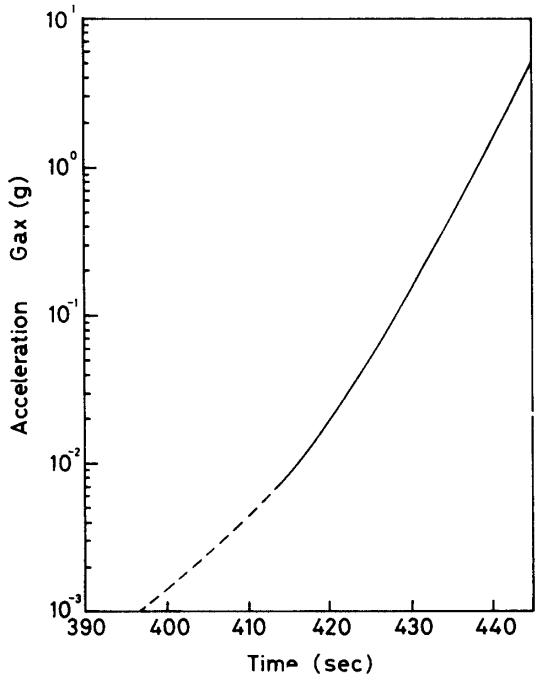

3-c. Reentry period.

Fig. 3. The axial component of acceleration during the second flight.

and at 377 sec, respectively. These actions produced only negligibly small axial acceleration component on the payload section, though they were evidently detected by the geomagnetic attitude sensor as the variations in the coning motion as shown in Fig. 2-b. The apogee was 223.2 km at 239.2 sec and the payload section splashed down at 455 sec for the second experiment. The data for the first were 329 km at 290 sec at the apogee, and at 565 sec, respectively. The positions of the pipes in the payload section were carefully chosen so that the effects of spin and coning motions

might be as small as possible. In fact, the largest value of the induced acceleration was $2\times 10^{-2}g_0$ at the pipe wall for 2.2 Hz of spin, which acted on the liquid perpendicularly to the pipe axis. Axial component of the acceleration resulted from coning motion was less than $10^{-3}g_0$. The second heat pipe experienced zero-g situation, in practical sense, about 400 sec, when any components of the acceleration were below $10^{-3}g_0$. The effect of the re-entry beginning about 410 sec on the axial component was considerably large as seen in Fig. 2-b and 3-c.

Most of the data including the heat pipe experiment were transmitted by a PCM telemetry whose transmitting capability was 200×64 words/sec.

3. Experimental Heat Pipes

The specification of the second heat pipe is given in Table 1. Both first and second pipes are 10 mm OD and 300 mm long circular pipes with 20 rectangular axial grooves (Fig. 4). The first differed from the second in the working fluid, which was 0.58 *g* of ammonia, and in the pipe material; aluminum A1050. The liquid charge, 3.9 scc, was apparently overfilled, and led to a formation of a liquid column in the pipe under such large acceleration condition as in one-g test. The total volume of the grooves was 3.0 cm^3. The pipe had nine thermistors mounted along the wall, T_1 through

Table 1. Specification of Second Heat Pipe

Pipe Material	Aluminum Alloy A6063
Dimension (mm)	10 (OD) by 300 (length)
Axial Grooves (mm)	0.5 (width) by 1.0 (depth) 20 grooves
Working Fluid	Freon 11, 5.6 g (3.9 scc)
Heat Sink	
Condenser	Finned
PCM Heat Sink	N-eicosane ($C_{20}H_{42}$)
Total Heat Capacity	73800 J
Melting Point	34°C

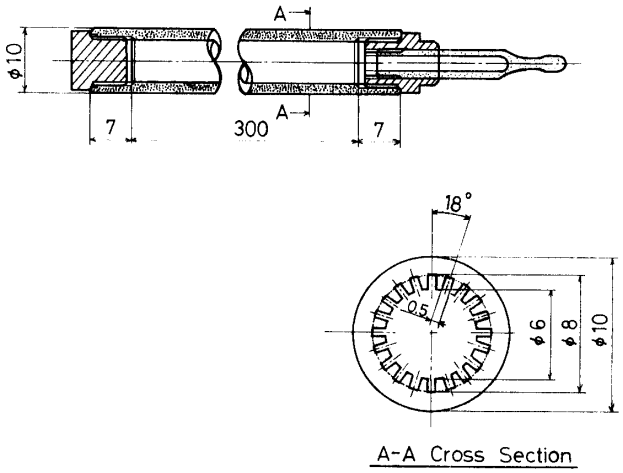

Fig. 4. The structure of the heat pipe for both flight experiments.

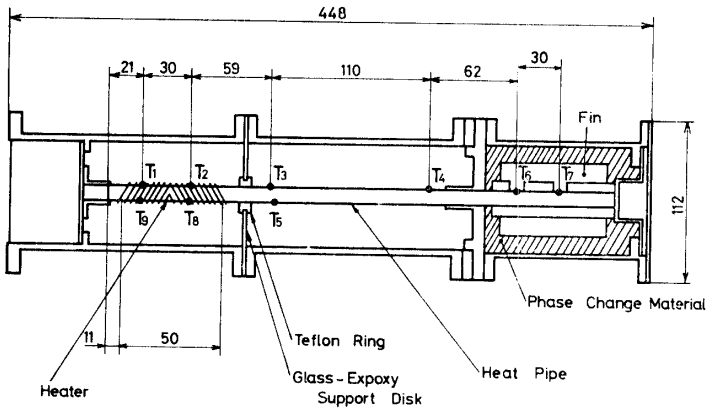

Fig. 5. The heat pipe instrumentation and assembly.

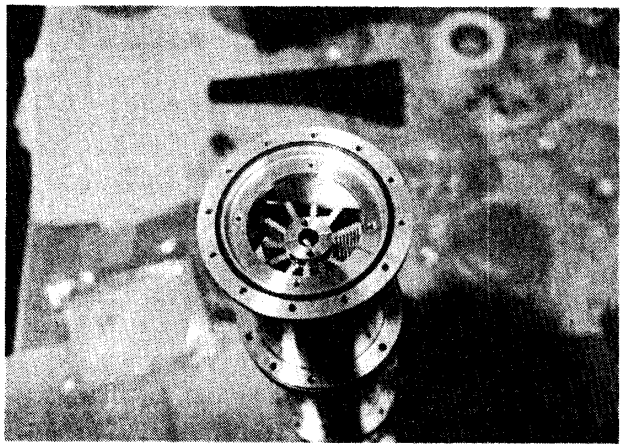

Fig. 6. Picture of heat sink section.

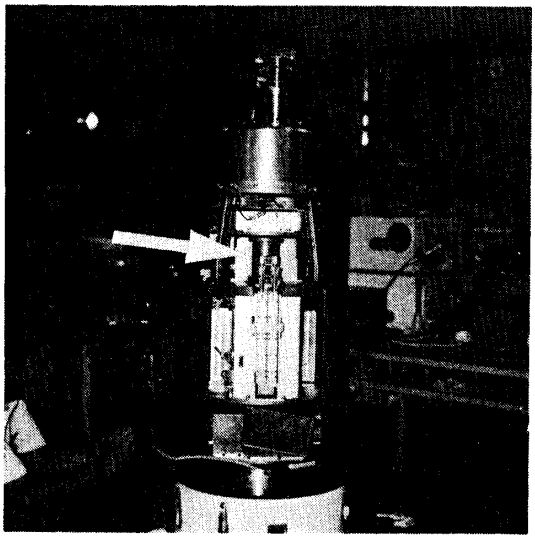

Fig. 7. The payload section assembly: The arrow indicates the top portion of the heat pipe capsule.

T_9, one of which, T_9, worked as the overheat detector in the evaporator, and a manganin heater winding as illustrated in Fig. 5. The aluminum condenser fins were employed in order to increase the heat transfer area to the phase change material (PCM), N-eicosane, in the heat sink section (Fig. 6). The pipe was supported by thermal insulating material, teflon rings and glassfiber-reinforced-epoxy disks, in an aluminum capsule, which was lined with multi-layer insulator. The capsule was not air tight, and air was evacuated to improve the thermal insulation as the rocket rose. This was installed with the condenser top on the rocket axis to avoid the influence of undesirable spin and coning motions (Fig. 7). The heat capacity of the PCM was as large as 73800 J, which corresponded to 50-min-heating at 24 *W*.

4. Ground Test Data

The heat pipe performance for the second experiment was checked in our lab in the same configuration as the flight one using N-eicosane PCM heat sink during conducting the preflight test. The axial temperature distributions are presented in Fig. 8 for vertical case in the reflux mode and horizontal case. Steady heat pipe operations were attained for each heating condition, $Q=10$ *W*, 24 *W* and 30 *W*. The temperature difference between the evaporator and the condenser sections was slightly larger for the horizontal case than for the vertical one. The upper side of the evaporator sec-

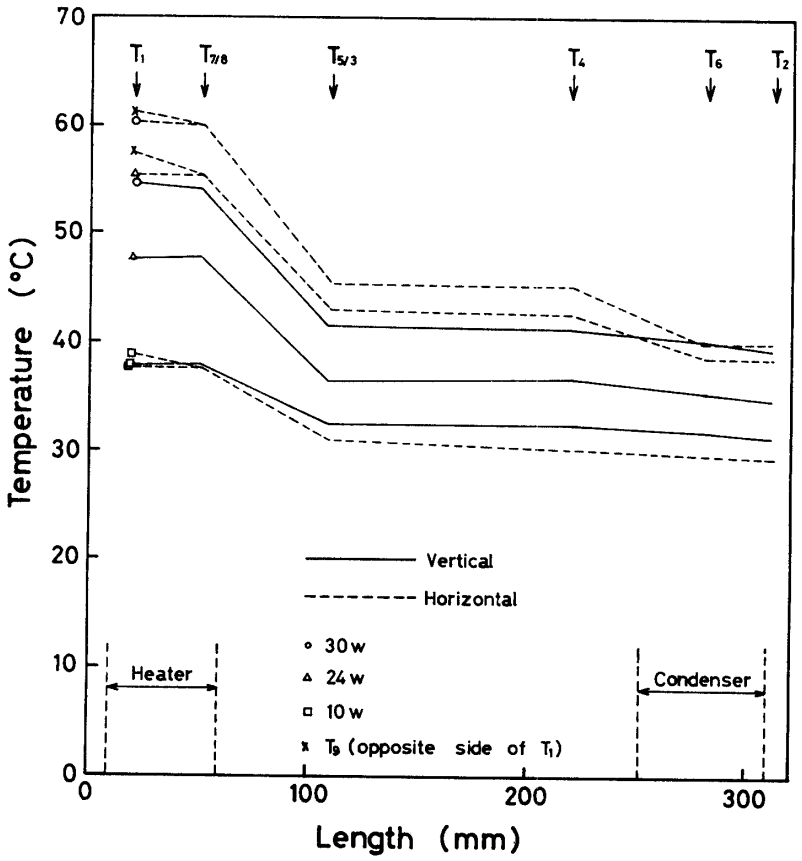

Fig. 8. Axial temperature distributions for horizontal and vertical cases.

tion for the horizontal case seemed to be in partial dryout state particularly at the end of the evaporator, T_9.

The transition to dryout situation is shown in Fig. 9 for horizontal configuration. The heat pipe was initially in steady operation mode for $Q=24$ W, and then the power was increased stepwise to 48 W. These two heating conditions were exactly same as the flight ones. It is evident from the rapid rise in T_1 that the dryout happened in the evaporator end for $Q=48$ W. The overheat protection circuit worked to switch off the heater at 72 sec.

The steady heat transfer performance is plotted in Fig. 10 for both vertical and

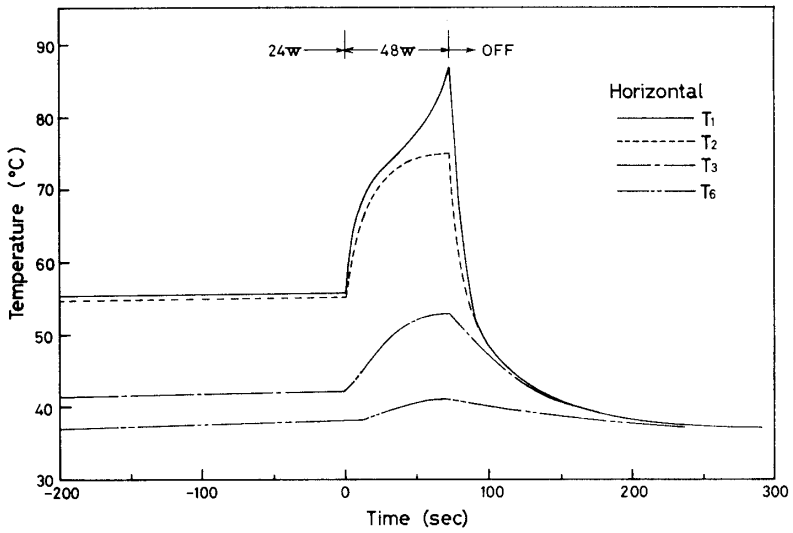

Fig. 9. Temperature history during transition to dryout.

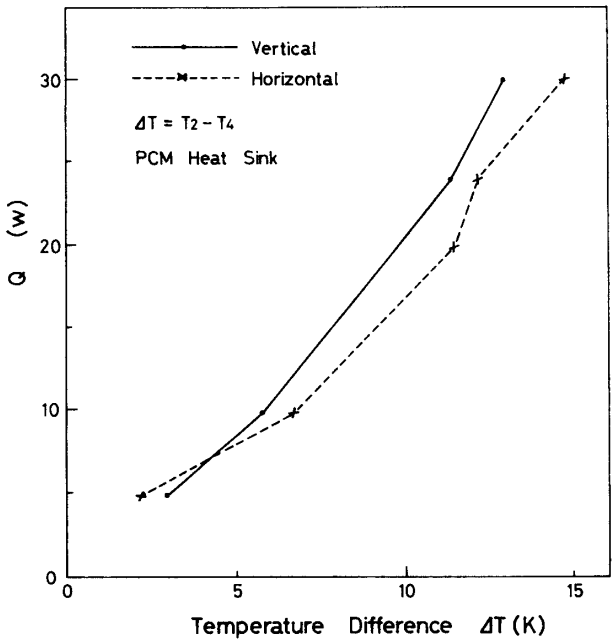

Fig. 10. Comparison of steady heat transfer performance between vertical and horizontal cases.

horizontal cases. The abscissa scale represents the temperature difference between the evaporator, T_2, and the adiabatic section, T_4. The heat transfer rate is roughly estimated to be 2 W/K for the freon 11 pipe. It was 3.5 W/K for the first (ammonia) pipe. The difference in these figures is considered to be resulted primarily from the difference in the thermophysical properties. In addition, the freon 11 pipe was apparently overfilled.

The effect of the acceleration on heat pipe performance was examined by varying the tilting angle. Fig. 11 shows the change in the temperature difference, $\Delta T = T_2 - T_4$, with the tilting angle, θ, for $Q = 24$ W, which is measured from the horizontal plane. The abscisssa is also scaled by the axial component of the gravitational acceleration, G_{ax}, in this figure. G_{ax} is taken to be positive for the reflux mode. The heat transfer performance changed only slightly for any positive values of θ, that is in the reflux mode, while it strongly depended on θ for the heat pipe mode and dryout occurred for $\theta = -0.7$ deg.

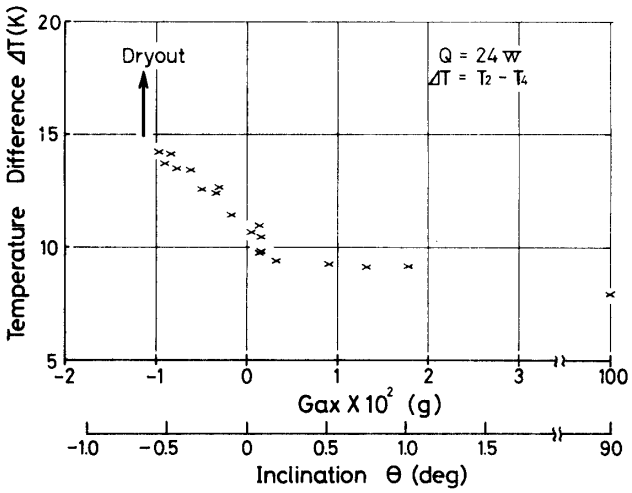

Fig. 11. Variation of temperatuse difference, ΔT, with tilting angle, θ.

The maximum heat transport capability is plotted against θ, or G_{ax}, in Fig. 12. At heating rates indicated by circles in this figure, steady operations were attained, while at those by crosses evaporator dryout was observed. The value $Q_{\max}$ would be found between the circles and the crosses in this figure. The theoretical $Q_{\max}$ is calculated by the formula given by Chi [8] for the case neglecting the hydrostatic pressure difference in the radial direction, $\Delta p_{\perp} = 0$:

$$Q_{\max} = \frac{1}{L_{\text{eff}}} \frac{2\sigma/r_c - \rho_l g_0 L_t \sin\theta}{F_l + F_v} \tag{1}$$

Where σ, ρ_l, r_c and L_t are the surface tension coefficient, the liquid density, the effective capillary radius or the groove half width, and the total length of the heat pipe, respectively. The effective length L_{eff} is defined in terms of the lengthes of the evaporator, L_e, the adiabatic section, L_a, and the condenser, L_c by

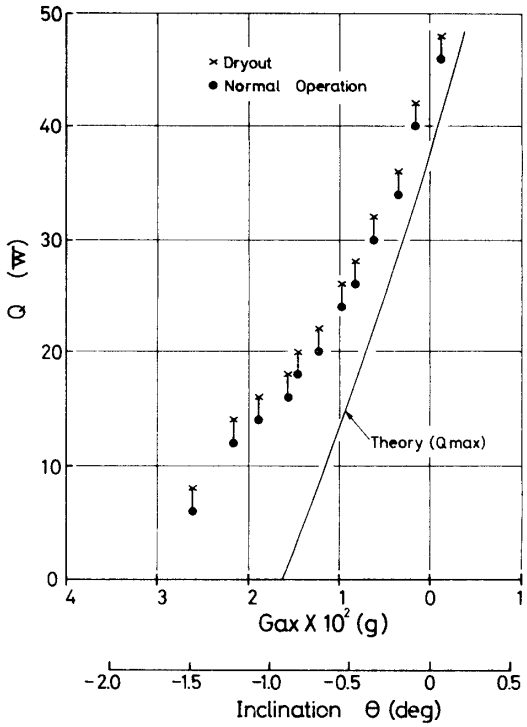

Fig. 12. Influence of the axial acceleration on the maximum heat transport capability.

$$L_{\text{eff}} = L_a + \frac{1}{2}(L_e + L_c). \tag{2}$$

The frictional coefficients F_l for the liquid flow and F_v for the vapor flow are written as follows,

$$F_l = \frac{\mu_l}{KA_w\rho_l\lambda}, \tag{3}$$

$$F_v = \frac{8\mu_v}{r_{h,v}^2 A_v \rho_v \lambda}. \tag{4}$$

Where μ_l, μ_v, ρ_v, λ are the viscosity of the liquid and the vapor, the vapor density, and the latent heat of vaporization, respectively. A_w and A_v are the total groove cross-sectional-area, and the vapor core cross-sectional area. The permeability K for the open rectangular grooves as in the present case is calculated from the formula;

$$K = \frac{2\varepsilon r_{h,l}^2}{(f_l \cdot R_{el})} \tag{5}$$

where ε is the porosity, and $r_{h,l}$ is the hydraulic radius for liquid flow defined in terms of the width w and the depth δ of a groove by

$$r_{h,l} = \frac{2w\delta}{w+2\delta}$$

The value of $(f_l \cdot R_{el})$ is usually given graphically as a function of the groove aspect ratio $w/2\delta$, which is presented in the text book [8]. In Eq. (4), the hydraulic radius for the vapor flow, $r_{h,v}$ is taken as the vapor core radius, $r_v = 3$ mm. Eq. (4) is a formula for laminar flow, and that is the case with the present heat pipe. The discrepancy between the experiment and the theory may be caused by liquid overfill, which promotes liquid supply to the evaporator even in the heat pipe mode because of the radialcomponent of the gravitational acceleration in one-g experiments. According to the experimental and theoretical results, the heat load, $Q = 48$ *W*, is just above $Q_{\max}$ in zero-g situation.

5. Flight Data

The heater was initiated about 20 min prior to the launch for both flight experiments so that the PCM partially melted in the vicinity of the condenser fins at the launch, when the rocket was set on the launcher at a zenith angle of 13.5 deg. The heating rate was constant, 24.2 *W*, during the first experiment, while it varyed sequentially for the second as shown in Fig. 13. The second pipe was heated at the rate $Q = 24$ *W* before launch, and then the power increased to 48 *W* at 123 sec. The heater was switched off by the action of the overheat protector at 130 sec. Such sequence was repeated 5 times. That is, the heater at $Q = 48$ *W* was turned on at 123 sec, 157 sec, 198 sec, 239 sec and 281 sec, while it was turned off at 130 sec, 174 sec, 214 sec, 257 sec and 298 sec. Finally, the 24 *W* heater was turned on at 356 sec after zero-heating period for 58 sec, and the heating rate was maintained untill the end of the flight.

The temperature history of the first flight experiment is shown in Fig. 14. Valid telemetry data were received until 243 sec, when the onboard power supply system was partially damaged by a failure of high voltage lines of the microwave experiment. The sensor T_5 monitored the ambient temperature on the outer wall of the aluminum capsule, which indicated 18.5°C throughout the experiment. The evaporator temperature went down by about 1.2 *K* subsequent to the launch compared with that

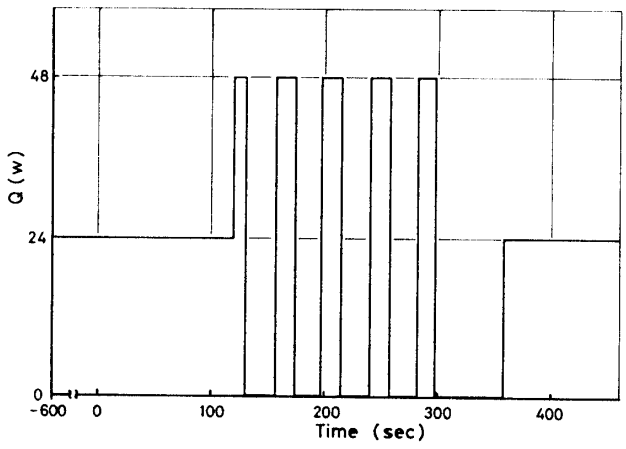

Fig. 13. Heating rate during the second flight experiment.

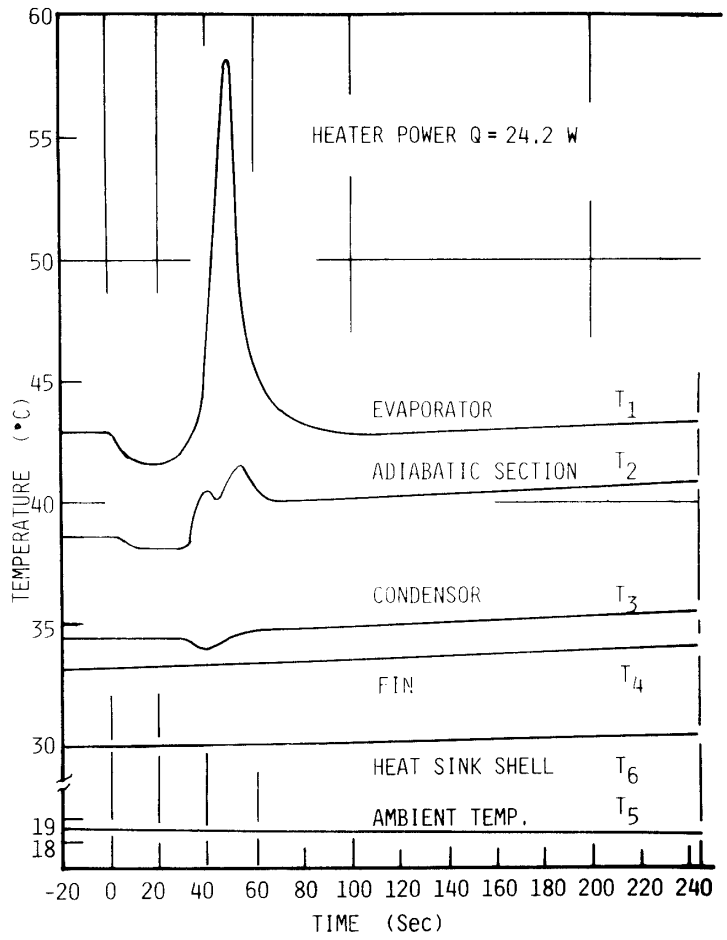

Fig. 14. Temperature history during the first flight experiment.

before launch. During this period the heat pipe experienced very large axial acceleration up to 18 g_0 in the reflux mode. This temperature drop may be attributed to the effect of large acceleration on boiling in the evaporator section. Even 30% of volumetric fill of the working fluid in grooves for this particular heat pipe resulted in forming a puddle in the evaporator section under such large acceleration condition. At 32 sec, an onset of dryout was detected, which precisely coincided with the burnout time. This was caused by negative axial acceleration produced as a result of the aerodynamic drag on the rocket. The altitude was about 35 km at the burnout where the atmospheric pressure was as high as to induce fairly large drag because of very large vehicle velocity. The dryout and possible formation of a liquid puddle in the condenser on this occasion were also detected through small temperature drop in the condenser, T_3. It is interesting to note that the record T_2 has two peaks. The first may be caused by the flow of bulk hot working fluid from the evaporator toward the condenser. The second may result from dryout. The normal heat pipe operation began to recover from dryout state after 47 sec, when any components of the acceleration became enough small ($<10^{-3}\ g_0$). In this operation mode, zero-g mode, the total temperature drop in the pipe decreased by about 0.7 K and the temperature

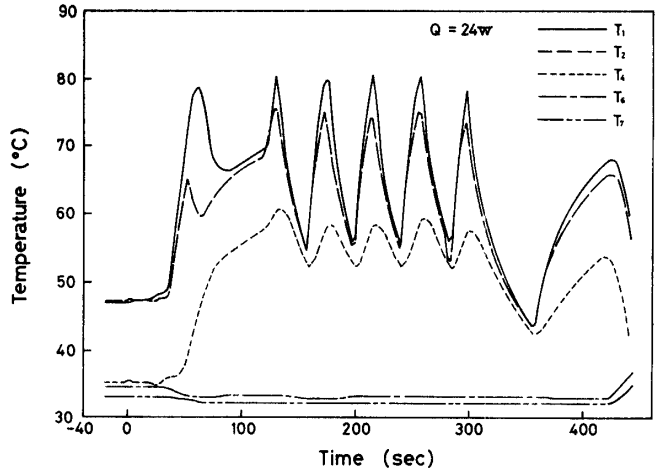

Fig. 15. Temperature history during the second flight experiment.

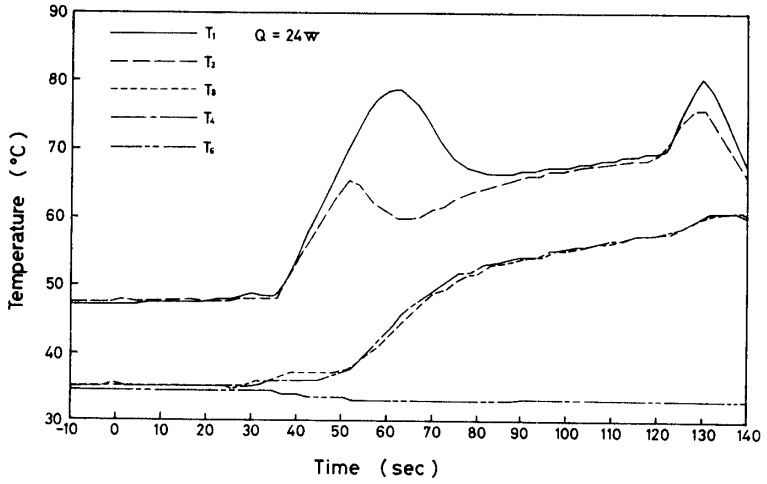

Fig. 16. Temperature history of the second experiment in the initial stage of the flight.

in the adiabatic section rose by 2 K compared with the one-g performance on the launcher.

For the second experiment, the temperature variations are presented in Fig. 15. The curves consist of the output from typical six thermistors among the nine, T_1 and T_2 in the evaporator, T_4 in the adiabatic section close to the condenser, T_6 and T_7 in the condenser (see Fig. 5). The time scale covers whole experimental period. Fig. 16 shows the variations in the initial stage of the flight from -10 sec through 140 sec, and Fig. 17 represents those in the final stage from 320 sec to the splash down. The variations well reflect thermal and dynamical responses of the heat pipe to the varying acceleration and the change of heating rate Q. At 32 sec, the pipe turned to dryout as the first heat pipe had done. The recovery from this state began at 44 sec as the rapid reduction of the axial component of the (negative) acceleration. However, the normal heat pipe operation was not realized again until the re-entry. It is satisfactory to consider that the liquid column formed in the condenser section by large

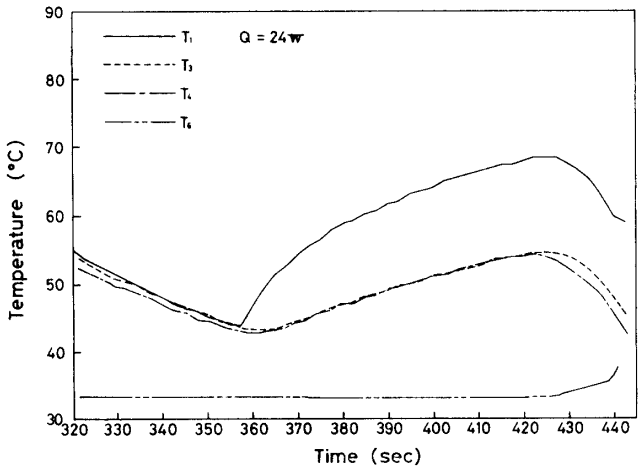

Fig. 17. Temperature history of the second experiment in the final stage of the flight.

negative acceleration did not completely disappear in the pseudo-zero-g state. It blocked the condenser section and prevented vapor condensation there. Therefore, the thermal resistance in the section considerably increased to result in temperature rise in the other sections. This will be discussed in more detail later.

The heater power increased to 48 *W* at 123 sec. This led the evaporator to dryout. The overheat protection, acted to switch off the heater at 130 sec. Such sequence was repeated 5 times, but no normal operations were observed for this heating rate. The pipe was left in zero-load condition for about one minute from 298 sec through 356 sec. The heater switched on again at 356 sec, but it seems that the liquid blockage did not yet disappear.

The normal heat pipe operation began to recover because of large (positive) axial acceleration during the re-entry as seen from Fig. 17, though a steady operation did not yet be realized before the splash down. The temperature in the evaporator and the adiabatic sections rapidly dropped and that in the condenser rose from 422 sec. It is considered that the liquid column was wiped off the condenser in this last stage.

Both heat pipe experiments did not recovered and thus no post flight data are available.

6. Discussion

An experiment had been conducted in the lab before the second flight in order to simulate the transient behavior resulted from the occurrence of negative acceleration, as such behavior had been anticipated as a result of the analysis of the first experiment. This experiment was carried out by changing the angle of the pipe axis measured from the horizontal plane by one deg in the heat pipe mode for first 40 sec. The heating power was kept constant, 24 *W*, throughout the experiment. The result given in Fig. 18 shows rapid dryout and subsequent recovery to normal heat pipe operation. The variation in temperature seems similar to the flight one from 32 sec through 80

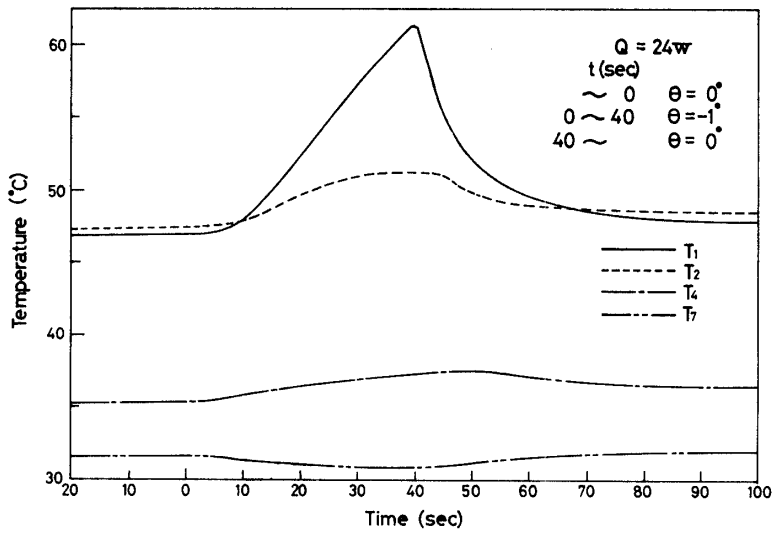

Fig. 18. Ground simulation test of dryout and recovery at constant heating rate Q=24 W.

sec as seen from Fig. 16. It should be noted that the manner of the temperature variation resulted from this test differs from that of the flight data from 80 sec through 120 sec and from 355 sec through 410 sec. In these two periods, the heat pipe did work, though significant portion of the condenser was blocked with liquid column. These different two situations can be readily distinguished by comparing the temperature difference between the evaporator and the adiabatic section, which is considerably larger for dryout. Such liquid blockage phenomena did not occur in the first heat pipe but normal heat pipe operation was recovered under zero-g condition. Liquid overfill is the most plausible cause to the blockage phenomena for the second experiment.

Another example of transient behavior was recorded during the re-entry started about 420 sec. As seen from Fig. 2-b and Fig. 3-c, the payload section set in rather complex motion, which is supposed to be a kind of autorotation. The period of such autorotation finally became less than 10 sec. Resulted axial component of the acceleration from such motion and the aerodynamic drag increased exponentially with time. Recovery to normal heat pipe operation started at 420 sec because of the axial (positive) acceleration, when the liquid column was pushed away the condenser toward the evaporator section. This can be well confirmed by the temperature variation T_6 illustrated in Fig. 17.

Bond number

The Bond number is frequently used to examine the nature of liquid behavior depending on whether the surface tension or the acceleration force dominates. This is defined as the ratio of the body force due to the acceleration to the surface tension force to be

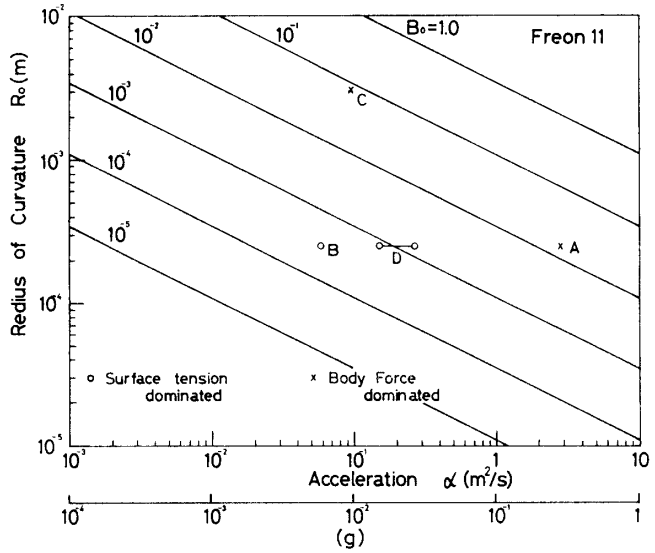

Fig. 19. The Bond number diagram for the second heat pipe experiment.

$$B_o = \frac{\rho \alpha R_0^2}{\sigma}, \tag{6}$$

where ρ is the liquid density, α the acceleration, R_0 the radius of curvature of free surface, and σ the surface tension coefficient. This is plotted for the second experiment in Fig. 19. For $B_0 \ll 1$, the surface tension dominates, while for $B_0 \gg 1$, the acceleration does. The half width of grooves, $w/2 = 0.25$ mm, or the radius of the vapor core, $r_v = 3$ mm, is chosen as R_0 for the present situation. In what follows, the Bond numbers are calculated corresponding to several events during the experiment. Firstly, onset of the liquid migration toward the condenser section because of negative acceleration is considered. Since the variation of the acceleration was so rapid to find the very instant of the onset, the acceleration is regarded as $-0.3\ g_0$ which is the maximum in this event. R_0 is 0.25 mm ($=w/2$). Thus, the Bond number upon the onset is computed to be 1.5×10^{-2}. This is marked by ***A*** in the figure. Of course, the magnitude should be less than $0.3\ g_0$ upon the onset of the liquid migration. The recovery from dryout started at 44 sec is denoted by ***B*** there, when R_0 was still $w/2$ and $|\alpha| = 6 \times 10^{-2}\ g_0$. This must be in the surface tension dominated region. A transition to the normal heat pipe operation due to the re-entry began at 416 sec, which is marked by ***C***, for which R_0 is taken to be r_v instead of $w/2$, and $\alpha = 1 \times 10^{-2}\ g_0$. This is obviously the acceleration dominated case. The Bond number roughly estimated by the data in the tilting test on the ground given in Fig. 12 is also indicated by ***D***. These data together with those from the first experiment are rearranged according to the Bond number in Fig. 20. It should be noted that the working fluid employed in the first heat pipe was ammonia whose ρ/σ value is less than half of that for freon 11. By the symbols ***A***, ***B*** and ***D*** for the first experiment were the same events meant as in the second. It may be concluded from these results that the critical Bond number giving the threshold of the surface tension dominated condition over the body force is about 5×10^{-3} for such configuration.

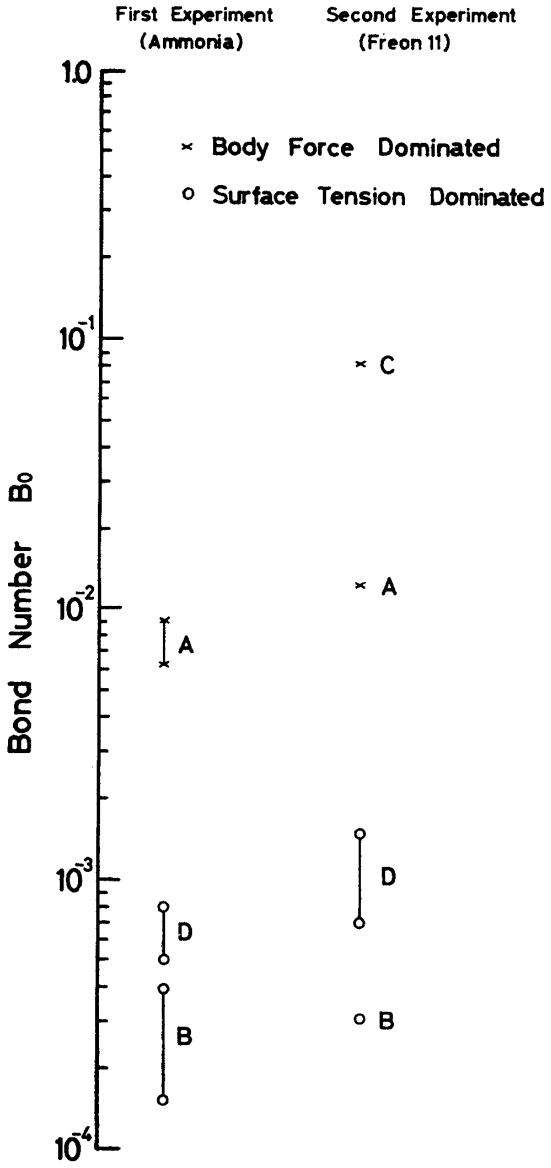

Fig. 20. Comparison of the Bond number between the the two flight experiments.

Marangoni effect

It is well known that the variation of surface tension gives rise to a tractive force on the surface [9, 10]. Such variation is readily resulted from temperature changes along the surface. This effect may make the liquid in the evaporator flow toward the condenser, and may bring about capacity degradation or dryout in the worst case. Thus, an estimate is carried out related to possible contribution of this effect on the peculiar behavior from 80 sec through 120 sec. It is convenient way doing this to evaluate the dynamic Bond number defined by [10].

$$B_d = \frac{\rho\alpha\delta\bar{L}}{\sigma_T(T_H - T_c)}. \tag{7}$$

Where it is considered for the liquid configuration that the liquid depth is the groove

depth δ, the reference length $\bar{L}$ which is the extent of the surface temperature distribution along the groove is 10 cm and that the acceleration α is acting in the same direction as the temperature variation. The temperature difference $T_H - T_c$ between the highest and the lowest is assumed to be 10 K. The temperature derivative of the surface tension, σ_T, is calculated to be -1.3×10^{-4} (N/mK) at 40°C. Then, the dynamic Bond number is found to be 1.1, which should be rather conservative estimate. This magnitude of B_d indicates that the effect is not so large to sweep the liquid off the evaporator to turn into dryout. In fact the situation was not in dryout condition. For this effect to be significant, the term $\sigma_T(T_H - T_c)/\bar{L}$, which is equivalent to the spatial gradient of surface tension, should be enough large as found in the vapor-gas interface region in variable conductance heat pipes [9].

7. Conclusion

The results from two flight experiments may be summarized as follows:

i) Axial grooved heat pipes are very sensitive to the variation of axial component of the acceleration.

ii) The critical Bond number giving the threshold of the surface tension dominated condition over the body force is about 5×10^{-3}.

iii) Liquid overfill may give rise to liquid blockage in the condenser section in zero-g, which can not be reproduced in one-g situation.

iv) The Marangoni effect is not so large for heat pipes without noncondensible gas.

Acknowledgement

The authors would like to express cordial thanks to Professor T. Horiuchi, ISAS and Mr. S. Terai, Director of Sumitomo Light Metal Laboratory for their support to provide various kinds of heat pipes, and to Mr. R. Ohshima, Daicel Ltd. for providing heat sink material.

References

[1] Deverall, J. E., Salmi, S. W. and Knapp, R. J., "Heat Pipe Performance in Zero Gravity Field". J. Spacecraft and Rockets, Vol. 4, No. 11, 1967.

[2] Harwell, W., Edelstein, F., McIntosh, R. and Ollendorf, S., "OAO Heat Pipe Flight Performance Data", AIAA Paper 73-758, 1973.

[3] Kirkpatrick, J. P., "Variable Conductance Heat Pipes", Proc. of 1st Int. Heat Pipe Conf., Paper 7-3, 1974.

[4] McIntosh, R., Ollendorf, S. and Harwell, W., "The International Heat Pipe Experiment", AIAA Paper No. 75-726, 1975.

[5] Harwell, W., Quadrini, J., Sherman, A. and McIntosh, R., "Cryogenic Heat Pipe Experiment: Flight Performance Onboard a Sounding Rocket", AIAA Paper No. 75-729, 1975.

[6] Galzin, F., "A Heat Pipe Flight Test aboard a Sounding Rocket", Proc. of 2nd Int. Heat Pipe Conf., ESA SP-112, Vol. 1, March 1976, pp. 621.

[7] Savage, C. J., Aalders, B. G. M., Mathieu, J. P. and Munzel, W. D., "Heat Pipe Experiment on ASTRO-8(ii)", Progress in Astro. and Aero., Vol. 70, 1980.
[8] Chi, S. W., "Heat Pipe Theory and Practice", Hemisphere Publ. Co., 1976.
[9] Eninger, J. E., "The Marangoni Effect and Capacity Degradation in Axially Grooved Heat Pipes", Proc. of 3rd Int. Heat Pipe Conf., 1978.
[10] Pimputkar, S. M. and Ostrach, S., "Transient Thermocapillary Flow in Thin Liquid Layers", Phys. of Fluids, Vol. 23, No. 7, 1980, pp. 1281.